Research article

Nicholas V. Proscia^a, Robert J. Collison^a, Carlos A. Meriles* and Vinod M. Menon*

Coupling of deterministically activated quantum emitters in hexagonal boron nitride to plasmonic surface lattice resonances

https://doi.org/10.1515/nanoph-2019-0136 Received May 6, 2019; revised August 8, 2019; accepted August 17, 2019

Abstract: The cooperative phenomena stemming from the radiation field-mediated coupling between individual quantum emitters are presently attracting broad interest for applications related to on-chip photonic quantum memories and long-range entanglement. Common to these applications is the generation of electro-magnetic modes over macroscopic distances. Much research, however, is still needed before such systems can be deployed in the form of practical devices, starting with the investigation of alternate physical platforms. Quantum emitters in two-dimensional (2D) systems provide an intriguing route because these materials can be adapted to arbitrarily shaped substrates to form hybrid systems wherein emitters are near-field-coupled to suitable optical modes. Here, we report a scalable coupling method allowing color center ensembles in a van der Waals material (hexagonal boron nitride) to couple to a delocalized high-quality plasmonic surface lattice resonance. This type of architecture is promising for photonic applications, especially given the ability of the hexagonal boron nitride emitters to operate as single-photon sources at room temperature.

^aNicholas V. Proscia and Robert J. Collison: These authors contributed equally to this work

*Corresponding authors: Carlos A. Meriles and Vinod M. Menon,
Department of Physics, CUNY-City College of New York, New York,
NY 10031, USA; and Department of Physics, CUNY-Graduate Center,
New York, NY 10016, USA, e-mail: cmeriles@ccny.cuny.edu.
https://orcid.org/0000-0003-2197-1474 (C.A. Meriles);
vmenon@ccny.cuny.edu (V.M. Menon)

Nicholas V. Proscia: Department of Physics, CUNY-City College of New York, New York, NY 10031, USA; and Department of Physics, CUNY-Graduate Center, New York, NY 10016, USA

Robert J. Collison: Department of Chemistry, CUNY-City College of New York, New York, NY 10031, USA; and Ph. D. Program in Chemistry, The Graduate Center of the City University of New York, New York, NY, 10016, USA.

Keywords: defect; hexagonal boron nitride; surface plasmons; surface lattice resonance; strain; quantum emission; 2D materials; coupling; photoluminescence; delocalization.

1 Introduction

Van der Waals materials in the form of thin sheets (1–50 nm) or single atomic layers have received a great deal of attention as a light source due to their unique mechanical, electronic and optical properties [1–4]. Particularly, their ability to conform and integrate with other material systems offer unprecedented control over their electronic and optical response [5–8]. Additionally, these material systems exhibit intriguing quantum phenomena both at the macro scale (e.g. room temperature quantum Hall effect [9], condensates [10], and superconductivity [11]) and at the nanoscale (e.g. single photon emission from color centers [12, 13], and excitons [14–17]). These features have given the scientific community new ways to explore quantum phenomena while setting the stage for novel devices.

From among the many van der Waals systems presently attracting attention, in this study, we focus on hexagonal boron nitride (hBN), a semiconductor featuring a wide band gap (of approximately 6 eV [18]) and high thermal conductivity [19]. This material can be used in a wide range of applications, from catalysis [20] to electronics (e.g. as a component for atomically-thin heterostructures [21, 22]). Its crystal lattice is isomorphic to graphene, with boron and nitrogen forming the basic elements for a honeycomb structure [23]. Recently, hBN was identified as the host of room temperature single photon emitters (SPE) associated with point defects in its crystal lattice. These SPEs possess properties that are needed in a single photon source (SPS), including high excitation and out-coupling efficiency, photon purity

and a low Debye-Waller factor [12]. While the exact nature of the defects remains unclear, the low material cost, room temperature operation, high photon count rates, spectral tunability and narrow linewidth make these emitters highly attractive for quantum technologies [24–31].

Recent studies have shown that hBN grown via chemical vapor deposition (CVD) can contain a high density of point defects that can be "activated" (i.e. transformed into a fluorescent state) either by thermal annealing or substrate-engineering [32, 33]. In this latter case, the emitter position (and, to some extent, the areal concentration [34]) can be controlled, thus providing opportunities for integration with photonic structures [35, 36].

Processing information with quantum emitters requires scalable methods for deterministically placing these emitters in integrated photonic circuits and subsequently coupling to structures that can direct, amplify, and potentially modulate the emitted photons. On the one hand, small ensembles of independent emitters coupled to a cavity have recently gained attention with an eye on applications in quantum memory storage and its ability to act as entangled systems [37, 38]. On the other hand, photonic structures, such as plasmonic surface lattice resonances (SLRs) supporting delocalized or propagating modes, provide one attractive route to establishing long-range interactions between electronically independent emitters so as to control emission directionality and intensity. The coupling of emitters to this class of photonic systems has recently attracted research attention due to its potential as tunable light sources and for compact lasing applications [39-45].

In this report, we focus on engineering the emission properties of room temperature SPSs in hBN by combining deterministic emitter activation and coupling to an optically active substrate. This is achieved by placing 20 nm-thick hBN flakes on silver nanopillar arrays that support the SLRs. Capitalizing on the unique mechanical properties of the 2D materials, we activate the quantum emitters located in a target area by suitably shaping the underlying substrate [7, 8, 32], and subsequently engineering their emissions both directionally and spectrally with the aid of array-supported SLR modes [39]. While the exact mechanism by which the hBN emitters are activated has not been currently isolated, a likely candidate is the strain caused by the folding of the hBN around the nanopillars, which in turn, would lead the emitter into a bright radiative state [7, 8, 32, 46]. The number of emitters can be controlled via the size of the activated area and the intrinsic defect density [33].

2 Materials and methods

2.1 Sample preparation fabrication

In our experiments, we start with the fabrication of arrays of silver nanopillars via e-beam lithography. To this end, a PMMA film (positive resist) was patterned onto a glass substrate to produce regular, square arrays of cylindrical holes of variable diameter and separation (pitch). Then, a 100 nm layer of Ag was deposited on the patterned PMMA film via electron beam evaporation. Afterwards, a lift-off process was used to remove the Ag-coated PMMA via acetone, leaving behind arrays of silver nanopillars with different diameters and inter-site separations. Subsequently, a 10 nm conformal coating of alumina was deposited on the sample in order to passivate the Ag structure as well as to provide the spacing required to prevent silver-induced emitter quenching. To study the interaction between the hBN emission and the plasmonic arrays, we fabricated pillar structures with pitches varying from 220 nm to 2000 nm and with pillar diameters from 50 nm to 400 nm for each pitch. Generally, pillar arrays with a pillar-to-pillar spacing of less than 100 nm were found to fuse together, hence imposing a practical limit in the type of systems we could probe. Each array was 50×50 μm² in size, large enough to allow for a collective SLR mode while still compatible with the optical inspection.

The hBN used in the experiment was a CVD-grown 20 nm-thick film that was commercially available from Graphene Supermarket. The hBN flake had an approximate size of 5×5 mm², large enough to cover the entire patterned area with a continuous film. The hBN was deposited on the Ag pillar substrate via a wet transfer protocol described in Ref. [32].

2.2 Optical characterization

In order to obtain angle-resolved spectra in Figures 1 and 4, the Fourier image of the sample was projected onto the spectrometer slit (Princeton Instruments SpectraPro HR 750). The white light was focused on the array through the excitation objective (Exc. Obj.) and the transmitted light or PL was collected by the collection objective (Coll. Obj.) The collimated transmitted light was then focused by a tube lens (TL) to form a real image plane (IP) that was one focal distance away from the Bertrand lens (BL), which forms an image of the collection objective's back focal plane at the spectrometer slit (Det.) [47]. In this configuration, the spectrometer captures the Fourier image of the Ag pillar

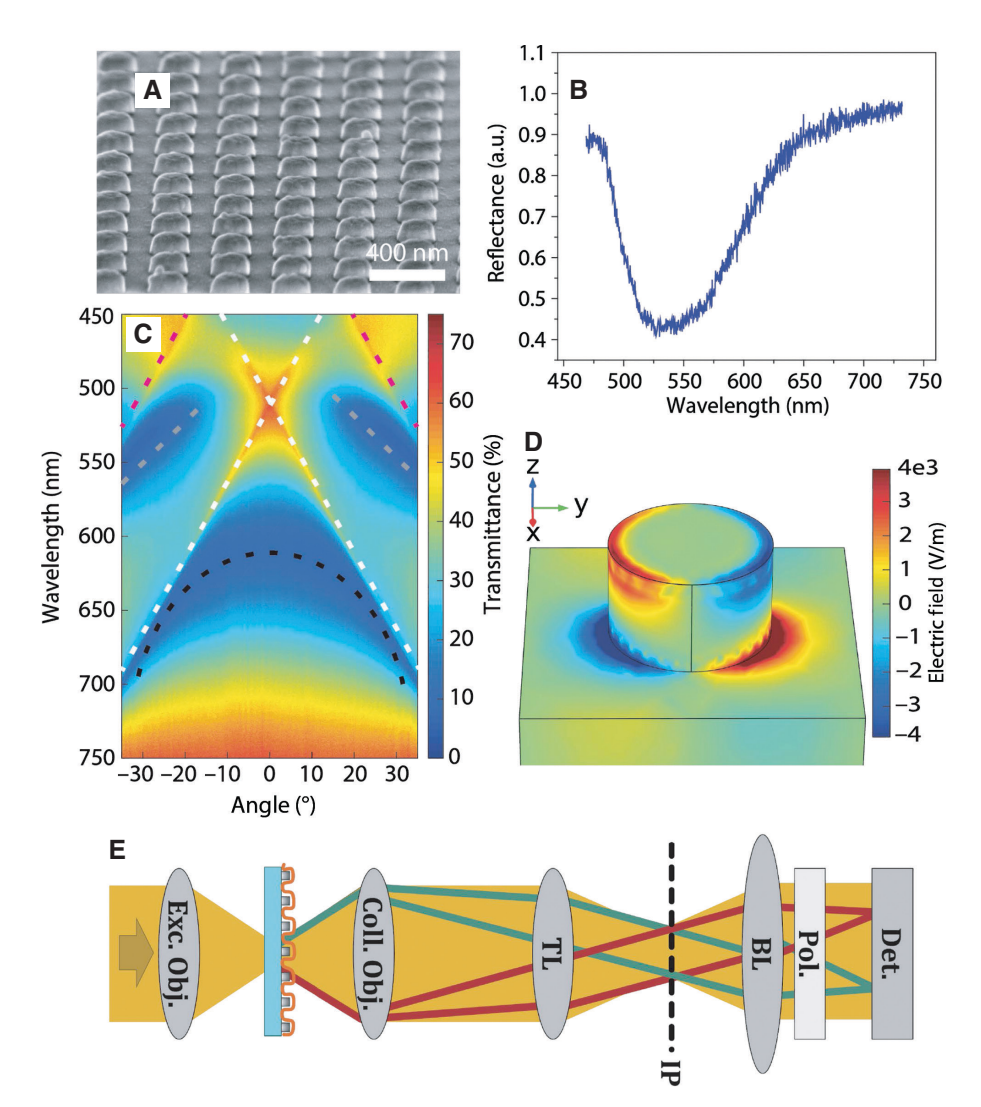


Figure 1: Ag nanopillar arrays and supported optical modes. (A) A tilted scanning electron microscopy (SEM) image of a bare array of silver nanopillars (345 nm pitch and 150 nm pillar diameter). (B) Reflectance spectrum from a single pillar from a confocal collection spot. (C) The measured angle-resolved transmission spectrum of the pillar geometry in (A) for p-polarized transverse magnetic (TM) incident light. White and red (black and grey) dotted lines corresponding to the RA (SLR) modes. (D) The simulated E,-field mode plot for the array in (A) of the out-of-plane SLR mode at an angle of 25° and wavelength of 655 nm. (E) The schematic diagram showing the Fourier microscope used to capture the angle-resolved spectra in (C) and Figure 4. The Bertrand lens (BL) is placed after the tube lens (TL) to form an angle-resolved (signified by the green and red traces) Fourier image at the slit of the detector (spectrometer).

array, where the linear polarizer (Pol.) is used to resolve the p- and s-polarizations. For the angle-resolved transmission spectra, the sample was illuminated via a tungsten lamp (Olympus) with a 0.6 NA long-working-distance objective (Olympus SLMPLN100x). For the photoluminescence spectra in Figure 4, a beam size of ~40 µm was used to excite the majority of the pillars in a given array.

Photoluminescence (PL) spectra were collected via a high numerical aperture (.83 NA) objective (Olympus). The confocal PL experiments in Figure 3 were performed with a custom-built confocal microscope. A piezo nanostage was used to raster scan the sample across a fixed laser and collection path. The focused spot size had a diameter of \sim 1 μ m and the collection spot was \sim 400 nm. The PL in Figure 3B was excited via a 510 nm, 500 fs pulsed fiber laser with a repetition rate of 80 MHz (Toptica FemtoFiber pro TVIS). The PL for the rest of the experiment was excited via a 460 nm CW diode laser.

3 Results and discussion

SLRs are hybrid plasmonic diffractive modes found in one- and two-dimensional periodic arrays of plasmonic

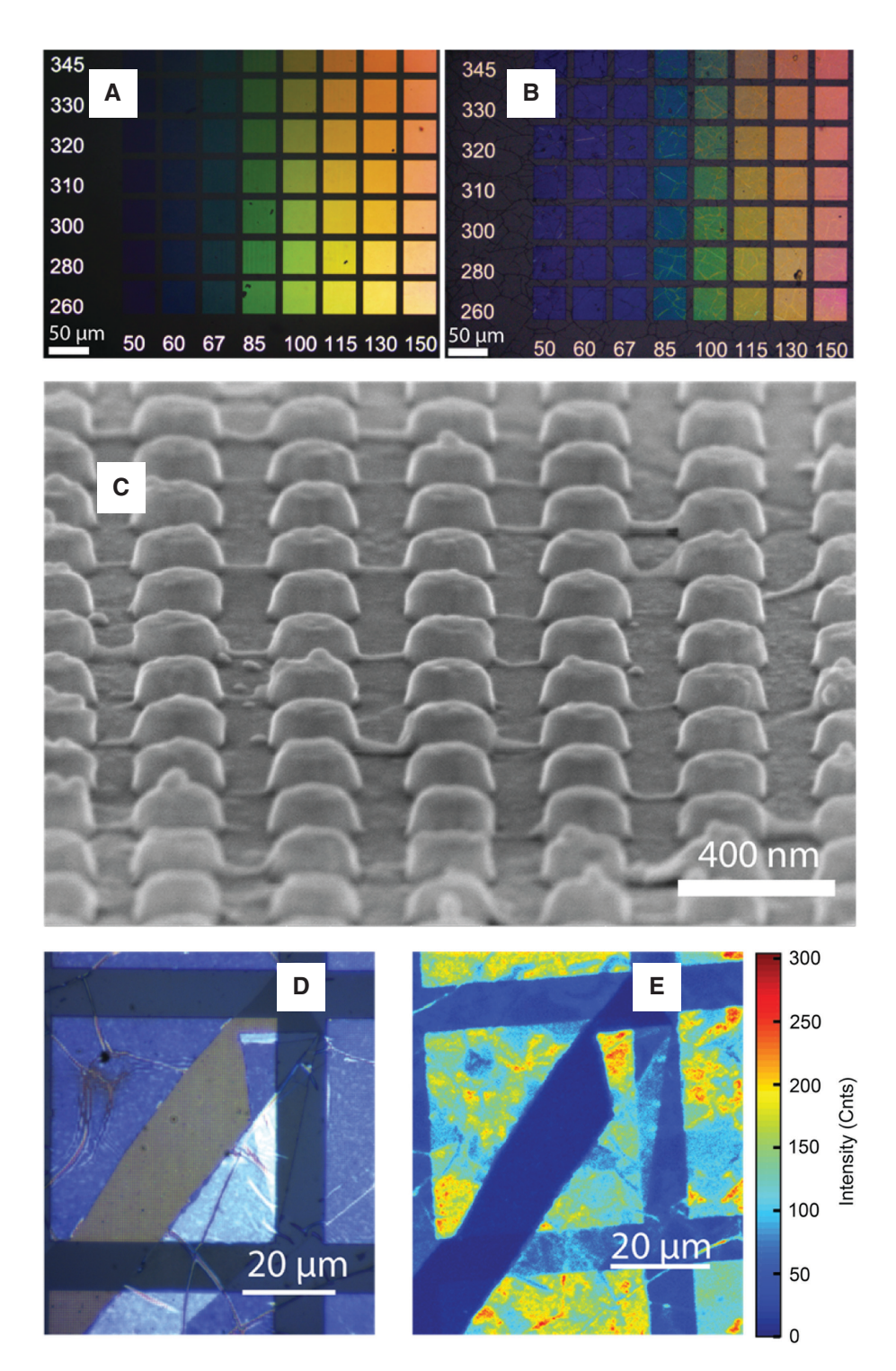


Figure 2: Ag nanopillar arrays capped with transfered hBN.

(A) The bright field optical microscopy image of various Ag pillar arrays on a glass substrate. The pitch increases vertically while the pillar diameters increase horizontally. The target sizes (in nm) are visible along the left and bottom sides of the patterned region. (B) Same as in (A) but after the transfer of a 20 nm-thick sheet of hBN. (C) The angled SEM image of the Ag pillar array covered with 20 nm hBN film. The hBN film takes the shape of the substrate without tearing. (D) The optical microscope image of partially torn hBN on the Ag pillar array having 150 nm diameter pillars and a 470 nm lattice period. (E) The confocal PL image of the same array as in (D).

nanoparticles. They are formed by the coupling of the localized surface plasmon resonances (LSPRs) of the discrete metal particles to in-plane diffraction orders known

as Rayleigh anomalies (RAs) [48]. Figure 1A shows an SEM image of a typical Ag nanopillar array recorded at a 70° tilt angle and a 30° scan rotation angle. It has a pitch of

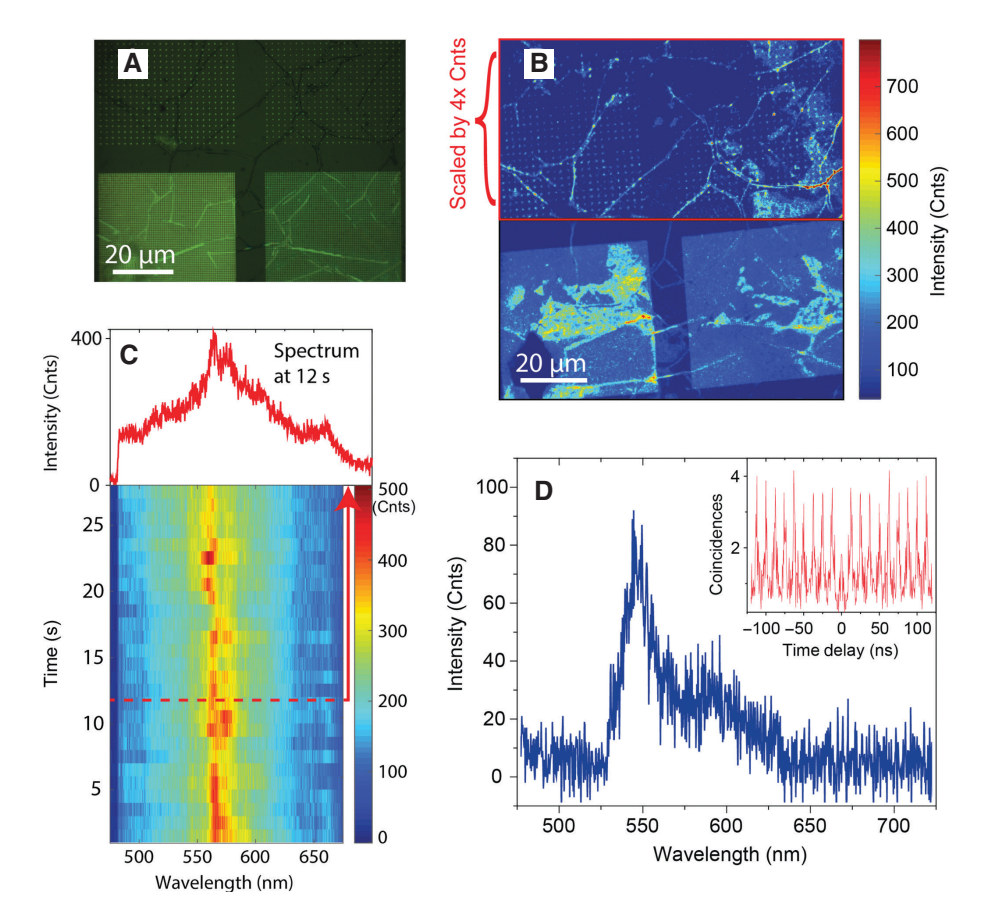


Figure 3: Confocal collection of emission of hBN on Ag pillars arrays.

(A) The optical microscope image of the hBN-draped Ag pillar arrays. The particle diameters are 400 and 300 nm for the pair of arrays in the left and the right halves, respectively; the arrays in the upper and lower halves have a lattice period of $2 \mu m$ and 620 nm, respectively. (B) The hBN photoluminescence for the same region as in (A). For clarity, we use different color scales for the arrays in the upper and lower halves. (C) The time-resolved emission spectra from a point on the array with 430 nm pitch and 100 nm pillar diameter. Several emitters are seen alternating between the bright and dark states in the 550-675 nm spectral band. The upper spectrum (red trace) corresponds to a line cut at 12 s. (D) The spectra from an isolated 100 nm-diameter pillar from a 2000 nm-pitch array. The phonon sideband is clearly visible ~165 eV from the zero-phonon line at 550 nm (blue trace). Inset: The photon correlation data via a pulsed Hanbury-Brown-Twiss measurement; an autocorrelation value $g^{(2)}(0) = 0.54$ was determined from the curve, implying 2 or less emitters.

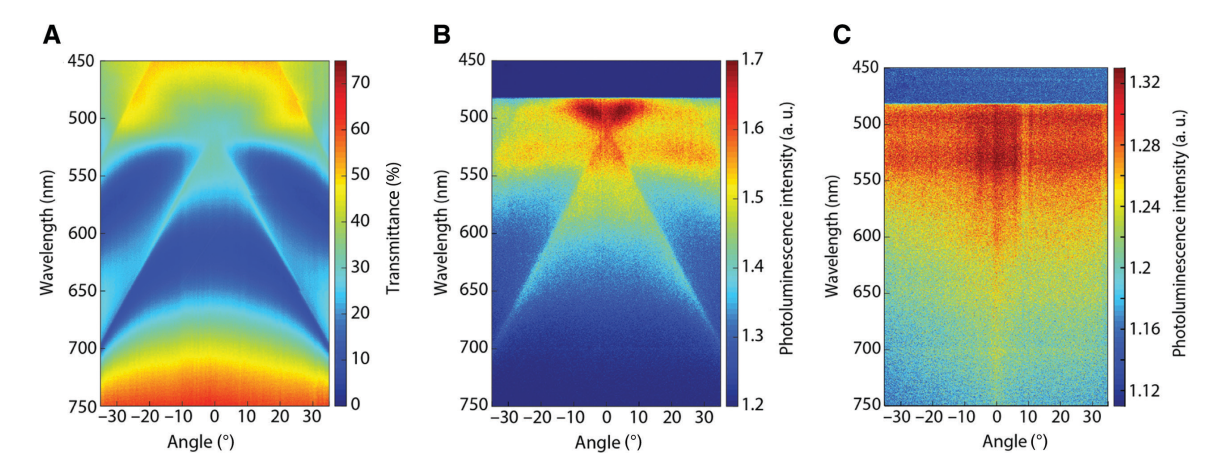


Figure 4: Angle-resolved spectra of Ag arrays with hBN.

(A) The transverse magnetic (TM) transmission spectrum of 345 nm-period/150-nm-pillar-diameter array studied in Figure 1 but with overlaid hBN. (B) The coupled PL from the hBN film on the same array with illumination from a 460 nm CW diode laser. (C) The angle-resolved PL spectrum from hBN on the 2000 nm pitch array with 150 nm diameter pillars. The SLRs in the visible wavelength range are not supported due to the large spacing between the pillars.

345 nm and a pillar diameter of 150 nm. As seen from the SEM image, the pillars are slightly tapered at the top. This change in diameter can lead to broadening of the LSPR mode as it depends highly on the pillar cross section [39]. The hybridized SLR modes occur at wavelengths slightly red-shifted from the wavelengths of the RAs (the high transmittance lines crossing at ~510 nm in Figure 1C). The SLR is seen in the dispersive extinction feature from 575 nm to 700 nm. The SLR in Figure 1C probed with a broadband white source has a Fano-resonance line shape due to the interference between the scattered light from the SLR mode and the directly transmitted broadband light [49]. The relevant modes here are the so-called "out-of-plane SLRs" that correspond to the LSPRs predominantly localized near the upper and lower ends of the pillars [50, 51].

For the geometry in Figure 1A, the non-dispersive LSPR mode for the 150 nm pillars, shown in Figure 1B, splits into two branches. The branch outside the 510 nm RA has two symmetrical lobes occurring between 500 nm and 560 nm centered at the original LSPR mode (indicated by the gray dotted lines in Figure 1C). These two lobes correspond to the SLR produced by the coupling of the Ag pillar LPSR to the higher energy $(0, \pm 1)_{air}$ RAs (red dotted lines). The lower energy $(0, \pm 1)_{glass}$ RA modes (white dotted lines) couple to the LSPR such that the resulting SLR (black dotted line) is continuous across normal incidence and follows the dispersion of the RA angles with gradually decreasing linewidths at larger angles. This is the typical behavior of SLRs [50]. Moreover, the quality of the mode increases at larger angles as these modes are longer lived when they become less localized at the individual Ag pillars.

The bright field microscope images of the Ag pillars arrays in Figure 2 allow us to compare the SLR's optical properties before and after hBN transfer. Aside from a ~20 nm red shift of the modes (expected from the higher index of the hBN film) and a slight decrease in the resonance quality, we find the SLRs were largely unaffected by the hBN film and retained all its core features. We fabricated Ag arrays with variable pitch and pillar diameter as seen in Figure 2A and B. This allowed us to study a large variety of SLR resonances as the hBN color centers occur across most of the visible spectrum, centered at ~570 nm [32, 52]. The 345 nm-pitch, 150 nm-pillar-diameter array was found to have the highest emission contrast on and off the SLR. Figure 2E shows a confocal scan of the observed PL. The hBN shows preferential emission when on the pillar array regions, while in the partially torn regions (seen in Figure 2D) the PL intensity was drastically reduced, indicating that the hBN was the source of the observed PL.

Figure 3 displays the emission characteristics of these hybrid hBN/Ag arrays. The hBN-induced

photoluminescence from isolated plasmonic particles was highly localized to individual pillars, as seen in the upper quadrants of Figure 3A and B. These arrays have a 2 µm spacing and do not support collective SLRs. The pillar locations of all four arrays are clearly identifiable in the bright field image of Figure 3A. At each pillar site, we can probe individual (or few) emitters as the pillar diameter is made sufficiently small [32]. For illustration purposes, Figure 3D shows a spectrum for a 100 nm-diameter pillar with 2 or less defects ($g^{(2)}(0) < 0.54 \pm 0.04$). The $g^{(2)}(0)$ was determined from the autocorrelation data in the inset of Figure 3D by taking the ratio between the area under the coincidence peak at t=0 and the average area of 10 $t\neq 0$ peaks. The area was determined by fitting each peak with a Lorentzian function [30]. Arrays that support SLRs (lower quadrants in Figure 3A) become collectively bright as seen in the confocal image of Figure 3B. As the pitch decreases, emitters get closer to each other and the collected fluorescence contains contributions from several defects. The latter leads to a broad dynamical emission across most of the visible spectrum (line cut in Figure 3C) with emitters blinking intermittently on a timescale of seconds (contour plot in Figure 3C).

To study the interplay between the emitter fluorescence and the SLRs, we look at the optical characteristics of the hBN-covered array already characterized in Figure 1. Aside from the slight changes pointed out above, the optical transmission spectrum in Figure 4A shows that the modes remain largely unaltered. By contrast, the blue laser excitation of the entire array (40 µm spot size) shows that the hBN emission is drastically modified via coupling into the SLR modes (Figure 4B). In particular, we observed that the PL becomes highly directional, largely mirroring the RA-induced SLR dispersion at high angles [39]. Moreover, the emission spectral band is extended by the SLR mode into the deep red, where the intensity of the defect emission is otherwise an order of magnitude weaker (red spectra of Figure 3C). These findings demonstrate good coupling between the defect center emission and the SLR modes. In the absence of an SLR mode (Figure 4C), the hBN emission shows no dispersion. This contrast with Figure 4B confirms that the dispersion of the hBN emission in Figure 4B is derived from the coupling of the hBN emitters to the SLR mode, which is supported by the 345 nm pitch Ag nanopillar array.

4 Conclusions

In summary, we presented a method for engineering room temperature quantum emission in a scalable platform where the emitters are activated at the array sites via substrate engineering. For suitable array parameters, the defect emission couples to the optically active plasmonic substrate and undergoes a modification in its directionality and spectral intensity. The coupling of emitter systems with photonic structures that support delocalized or propagating modes permits the mutual interaction between these distinct and spatially separated color centers. Such structures could facilitate long range energy transfer between individual emitters. Future works could focus on controlling the number of emitters coupling to the SLR mode via the size of the active region; this can be done by considering the number of intrinsic defects present in the material or by conducting spectral filtering [33].

Acknowledgments: N.V.P. and V.M.M. acknowledge the support from the NSF MRSEC program (DMR-1420634) and the NSF EFRI 2-DARE program (EFMA -1542863). C.A.M acknowledges the support from the National Science Foundation (NSF-1619896 and NSF-1726573) and from the Research Corporation for Science Advancement through a FRED Award. All authors acknowledge support from and access to the infrastructure provided by the NSF CREST IDEALS (NSF Grant No. HRD-1547830). The fabrication and SEM work were performed at the Advanced Science Research Center Nanofabrication Facility of the Graduate Center at the City University of New York.

References

- [1] Liu Y, Weiss NO, Duan X, Cheng HC, Huang Y, Duan X. Van der Waals heterostructures and devices. Nat Rev Mater 2016:1:16042.
- [2] Koperski M, Molas MR, Arora A, et al. Optical properties of atomically thin transition metal dichalcogenides: observations and puzzles. Nanophotonics 2017;6:1289-308.
- [3] El-Kady MF, Shao Y, Kaner RB. Graphene for batteries, supercapacitors and beyond. Nat Rev Mater 2016;1:16033.
- [4] Schulman DS, Arnold AJ, Razavieh A, Nasr J, Das S. The prospect of two-dimensional heterostructures: a review of recent breakthroughs. IEEE Nanotechnol Mag 2017;11:6-17.
- [5] Liu X, Galfsky T, Sun Z, et al. Strong light-matter coupling in two-dimensional atomic crystals. Nat Photonics 2015;9:30-4.
- [6] Shepard GD, Ajayi O, Li X, Zhu X-Y, Hone J, Strauf S. Nanobubble induced formation of quantum emitters in monolayer semiconductors. 2D Mater 2017;4:021019.
- [7] Branny A, Kumar S, Proux R. Gerardot BD. Deterministic straininduced arrays of quantum emitters in a two-dimensional semiconductor. Nat Commun 2017;8:15053.
- [8] Palacios-Berraquero C, Kara DM, Montblanch ARP, et al. Largescale quantum-emitter arrays in atomically thin semiconductors. Nat Commun 2017;8:15093.
- [9] Novoselov KS, Jiang Z, Zhang Y, et al. Room-temperature quantum Hall effect in graphene. Science 2007;315:1379-9.

- [10] Debnath B, Barlas Y, Wickramaratne D, Neupane MR, Lake RK. Exciton condensate in bilayer transition metal dichalcogenides: Strong coupling regime. Phys Rev B 2017;96:174504.
- Cao Y, Fatemi V, Fang S, et al. Unconventional superconductivity in magic-angle graphene superlattices. Nat Publ Gr 2018;556:43-50.
- [12] Tran TT, Bray K, Ford MJ, Toth M, Aharonovich I. Quantum emission from hexagonal boron nitride monolayers. Nat Nanotechnol 2015;11:37-41.
- [13] Museur L, Feldbach E, Kanaev A. Defect-related photoluminescence of hexagonal boron nitride. Phys Rev B 2008;78:155204.
- [14] Tonndorf P, Schmidt R, Schneider R, et al. Single-photon emission from localized excitons in an atomically thin semiconductor. Optica 2015;2:347-52.
- [15] He Y, Clark G, Schaibley JR, et al. Single quantum emitters in monolayer semiconductors. Nat Nanotechnol 2015;10:497-502.
- [16] Srivastava A, Sidler M, Allain AV, Lembke DS, Kis A, Imamo A. Optically active quantum dots in monolayer WSe 2. Nat Nanotechnol 2015;10:491-6.
- [17] Koperski M, Nogajewski K, Arora A, et al. Single photon emitters in exfoliated WSe 2 structures. Nat Nanotechnol 2015;10:503-6.
- [18] Cassabois G, Valvin P, Gil B. Hexagonal boron nitride is an indirect bandgap semiconductor. Nat Photonics 2016;10:262-6.
- Golberg D, Bando Y, Huang Y, et al. Boron nitride nanotubes and nanosheets. ACS Nano 2010;4:2979-93.
- [20] Grant JT, Carrero CA, Goeltl F, et al. Selective oxidative dehydrogenation of propane to propene using boron nitride catalysts. Science 2016;354:1570-3.
- [21] Pan W, Xiao J, Zhu J. Biaxial compressive strain engineering in graphene/boron nitride heterostructures. Sci Rep 2012;2:893.
- [22] Geim AK, Grigorieva IV. Van der Waals heterostructures. Nature 2013;499:419-25.
- [23] Fang H, Bai SL, Wong CP. "White graphene" hexagonal boron nitride based polymeric composites and their application in thermal management. Compos Commun 2016;2:19-24.
- [24] Tran TT, Zachreson C, Berhane AM, et al. Quantum emission from defects in single-crystalline hexagonal boron nitride. Phys Rev Appl 2016;5:034005.
- [25] Jungwirth NR, Calderon B, Ji Y, Spencer MG, Flatté ME, Fuchs GD. Temperature dependence of wavelength selectable zerophonon emission from single defects in hexagonal boron nitride. Nano Lett 2016;16:6052-7.
- [26] Li X, Shepard GD, Cupo A, et al. Nonmagnetic quantum emitters in boron nitride with ultranarrow and sideband-free emission spectra. Acs Nano 2017;11:6652-60.
- [27] Vogl T, Lecamwasam R, Buchler BC, Lu Y, Lam PK. Compact cavity-enhanced single-photon generation with hexagonal boron nitride. ACS Photonics 2019;6:51.
- [28] Martínez LJ, Pelini T, Waselowski V, et al. Efficient single photon emission from a high-purity hexagonal boron nitride crystal. Phys Rev B 2016;94:121405.
- Tran TT, Wang D, Xu ZQ, et al. Deterministic coupling of quantum emitters in 2D materials to plasmonic nanocavity arrays. Nano Lett 2017;17:2634-9.
- [30] Grosso G, Moon H, Lienhard B, et al. Tunable and high-purity room temperature single-photon emission from atomic defects in hexagonal boron nitride. Nat Commun 2017;8:1-8.

- [31] Nguyen M, Kim S, Tran TT, et al. Nanoassembly of quantum emitters in hexagonal boron nitride and gold nanospheres. Nanoscale 2018;10:2267–74.
- [32] Proscia NV, Shotan Z, Jayakumar H, et al. Near-deterministic activation of room-temperature quantum emitters in hexagonal boron nitride. Optica 2018;5:1128–34.
- [33] Mendelson N, Xu ZQ, Tran TT, et al. Engineering and tuning of quantum emitters in few-layer hexagonal boron nitride. ACS Nano 2019;13:3132–40.
- [34] Javey A, Kang JS, Desai SB, et al. Strain-induced indirect to direct bandgap transition in multilayer WSe 2. Nano Lett 2014;14:4592-7.
- [35] Cai T, Kim JH, Yang Z, Dutta S, Aghaeimeibodi S, Waks E. Radiative enhancement of single quantum emitters in wse2 monolayers using site-controlled metallic nanopillars. ACS Photonics 2018;5:3466-71.
- [36] Luo Y, Shepard GD, Ardelean JV, et al. Deterministic coupling of site-controlled quantum emitters in monolayer WSe 2 to plasmonic nanocavities. Nat Nanotechnol 2018;13:1137–42.
- [37] Zhong T, Kindem JM, Rochman J, Faraon A. Interfacing broadband photonic qubits to on-chip cavity-protected rare-earth ensembles. Nat Commun 2017;8:14107.
- [38] Evans RE, Bhaskar MK, Sukachev DD, et al. Photon-mediated interactions between quantum emitters in a diamond nanocavity. Science 2018;362:662–5.
- [39] Vecchi G, Giannini V, Gómez Rivas J. Shaping the fluorescent emission by lattice resonances in plasmonic crystals of nanoantennas. Phys Rev Lett 2009;102:146807.
- [40] Guo R, Derom S, Väkeväinen AI, et al. Controlling quantum dot emission by plasmonic nanoarrays. Opt Express 2015;23:28206.
- [41] Zhou W, Dridi M, Suh JY, et al. Lasing action in strongly coupled plasmonic nanocavity arrays. Nat Nanotechnol 2013;8:506–11.

- [42] Yang A, Hoang TB, Dridi M, et al. Real-time tunable lasing from plasmonic nanocavity arrays. Nat Commun 2015;6:6939.
- [43] Wang D, Yang A, Wang W, et al. Band-edge engineering for controlled multi-modal nanolasing in plasmonic superlattices. Nat Nanotechnol 2017;12:889–94.
- [44] Hakala TK, Rekola HT, Väkeväinen AI, et al. Lasing in dark and bright modes of a finite-sized plasmonic lattice. Nat Commun 2017;8:13687.
- [45] Schwarz S, Kozikov A, Withers F, et al. Electrically pumped single-defect light emitters in WSe 2. 2D Mater 2016;3:025038.
- [46] Wang Y-T, Liu W, Li Z-P, et al. A bubble-induced ultrastable and robust single-photon emitter in hexagonal boron nitride. Arxiv Prepr 2019:1906.00493.
- [47] Kurvits JA, Jiang M, Zia R. Comparative analysis of imaging configurations and objectives for Fourier microscopy. J Opt Soc Am A 2015;32:2082.
- [48] Kravets VG, Kabashin AV, Barnes WL, Grigorenko AN. Plasmonic surface lattice resonances: a review of properties and applications. Chem Rev 2018;118:5912-51.
- [49] Auguié B, Barnes WL. Collective resonances in gold nanoparticle arrays. Phys Rev Lett 2008;101:143902.
- [50] Kravets VG, Schedin F, Grigorenko AN. Extremely narrow plasmon resonances based on diffraction coupling of localized plasmons in arrays of metallic nanoparticles. Phys Rev Lett 2008;101:087403.
- [51] Zhou W, Hua Y, Huntington MD, Odom TW. Delocalized lattice plasmon resonances show dispersive quality factors. J Phys Chem Lett 2012;3:1381-5.
- [52] Koperski M, Nogajewski K, Potemski M. Single photon emitters in boron nitride: more than a supplementary material. Opt Commun 2018;411:158–65.